Research Article

Effect of Cryogenic Treatment on the Microstructure Modification of SKH51 Steel

Kaweewat Worasaen
Mechanical Engineering (IDEME), The Sirindhorn International Thai-German Graduate School of Engineering, King Mongkut's University of Technology North Bangkok, Bangkok, Thailand

Piyada Suwanpinij[+]
Materials and Production Engineering (MPE), The Sirindhorn International Thai-German Graduate School of Engineering, King Mongkut's University of Technology North Bangkok, Bangkok, Thailand

Karuna Tuchinda*
Mechanical Engineering Simulation and Design (MESD), The Sirindhorn International Thai-German Graduate School of Engineering, King Mongkut's University of Technology North Bangkok, Bangkok, Thailand

* Corresponding author. E-mail: karuna.t@tggs.kmutnb.ac.th DOI: 10.14416/j.asep.2021.11.008
[+] Present address: Working Group Metallurgy and Metal Forming, Leibniz-Institut für Werkstofforientierte Technologien (IWT), Bremen, Germany
Received: 11 September 2021; Revised: 23 October 2021; Accepted: 4 November 2021; Published online: 23 November 2021

Abstract
This research aimed to investigate the microstructure modification mechanism used to improve the hardness and wear resistance of SKH51 steel. The cryogenic treatment (CT), including both shallow cryogenic treatment (SCT) and deep cryogenic treatment (DCT), was used to modify the microstructure of SKH51 steel in this research. The effect of short and long holding time (12 and 36 h) in CT was studied. The microstructures were evaluated by using a light optical microscopy (LOM) and a scanning electron microscopy (SEM). The phase identifications of the matrix, carbides, and a-parameter of the matrix were analyzed by using X-ray diffraction (XRD). The M_6C and MC carbides size, aspect ratio, and distribution were analyzed using digimizer image analysis software on the SEM micrographs. Micro-Vickers were employed to evaluate the hardness of the targeted samples. Wear tests were performed by using a 6 mm diameter WC ball as the indenter and 5-N-constant load with a ball-on-disk wear tester. The results suggested that the increase of the secondary carbide was caused by the contraction and expansion phenomena of the matrix's lattice, forcing the carbon atom out and acting as the carbide nucleation. The influence of holding time in the SCT and DCT regions was different. For the SCT, increasing the holding time increased the volume's fraction of MC carbide. Conversely, the M_6C carbide size grew with increasing holding time in the DCT region, while no significant increase in the number of MC carbide was observed. The cryogenic treatment was found to increase the volume fraction of the MC carbide by up to 10% compared to the conventional heat treatment (CHT) condition in the SCT region (both 12 and 36 h) and DCT with 12 h holding time. Due to the microstructure modification, it was found that the cryogenic treatment can improve material hardness and lead to an increase in the wear resistance of SKH51 by up to 70% compared to the CHT treated material. This was due to the increase in the compressive residual stress, precipitation of the MC, and growth of the M_6C primary carbide.

Keywords: SKH51 steel, Deep cryogenic treatment, Shallow cryogenic treatment, Carbide precipitation, Wear resistance

1 Introduction

Cryogenic treatment (CT) has been one process used for improving the mechanical properties of High-speed steels (HSS) such as hardness, toughness, wear resistance, and fatigue behavior [1], [2]. This technique was considered as a supplementary method for conventional heat treatment (CHT) to eliminate the retained austenite (RA) [3]. There are four major process parameters in CT including cooling rate, soaking temperature, soaking time, and heating rate during the process. Among the various parameters of CT, the soaking temperature has been found to have the greatest effect [4]. CT can be classified into three types based on process temperature: cold treatment, shallow cryogenic treatment (SCT) or subzero treatment, and deep cryogenic treatment (DCT) [5]. Cold treatment comprises microstructure refinement to achieve better static mechanical properties by treating materials in the temperature range of 0 to –80 °C. In SCT, the samples are treated in the temperature range of –80 to –180 °C in a medium, then exposed to room temperature. In DCT, the samples are slowly cooled to lower than –180 °C and held at that temperature for a desired duration, then gradually heated to room temperature to avoid cracking.

The application of CT is to promote the precipitation of fine secondary carbides, so increasing the carbide volume fraction, retained austenite transformation, η-carbide precipitation, and the homogeneity microstructure of the subjected tool steels [6], [7]. Accurate control of the process parameters, such as soaking temperature and time promotes the acquisition of superior mechanical properties. However, the main mechanism behind the improvements in the properties of materials after cryogenic treatment is still discussed among researchers [8], [9]. The correlation between microstructural alteration and mechanical properties is unclear, and the conducted investigations are sometimes contradictory. Many researchers have reported the benefit of DCT over SCT in wear resistance and tool life improvement [10]–[12].

Many research studies have endorsed the significance of the soaking temperature in augmenting various mechanical properties such as hardness, toughness, tensile strength, and wear resistance [13], [14]. The contribution of CT soaking temperature alone in improving the wear resistance of 18% Cr martensitic stainless steel was quantified as approximated 72% in Darwin's work [15]. Moore *et al.* [16] also worked on AISI T1 with variable soaking temperatures from –50 to –196 °C. It was observed that –100 °C is the optimal soaking temperature. Barron *et al.* [17] exposed samples of AISI T8 to varied soaking temperatures ranging from –73 to –196 °C and proposed that optimal results can be achieved at –196 °C. Mohan *et al.* [18] investigated different soaking temperatures for AISI T1 and AISI M2 and concluded that –180 °C results in a maximal improvement in wear resistance. Some researchers [19], [20] have proposed using –196 °C as the optimal soaking temperature for AISI M2, while Alexandru *et al.* [21] and Kelkar *et al.* [22] recommended –70 and –184 °C for the same material, respectively.

The understanding of microstructure modification due to CT in SKH51 (AISI M2 equivalent grade) steel, which is widely used in the tool and die industry would be useful. For this reason, this research aimed to study the effect of CT type on SKH51, i.e. the SCT and DCT temperature regions. The microstructure modification was investigated. The effect of the CT holding time for both CT temperatures will be disclosed. The hardness and wear resistance related to such microstructure change would be included. The research results could be used for such material improvement purposes.

2 Experimental Methods

2.1 *Materials preparation*

Molybdenum-HSS (SKH51) was analyzed in this research. Specimens were prepared in a cylindrical shape having 20 mm diameter and 5 mm thickness. The surface roughness (Ra) of all the samples was controlled to be approx. 0.5 μm by polishing. The chemical composition was investigated and is given in Table 1, as reported by optical emission spectroscopy (OES).

Table 1: Chemical composition of the SKH51 (%wt)

	C	Si	Mn	Cr	W	Mo	V	Fe
SKH51	0.9	0.3	0.4	4.2	6.5	5.0	2.0	Bal.

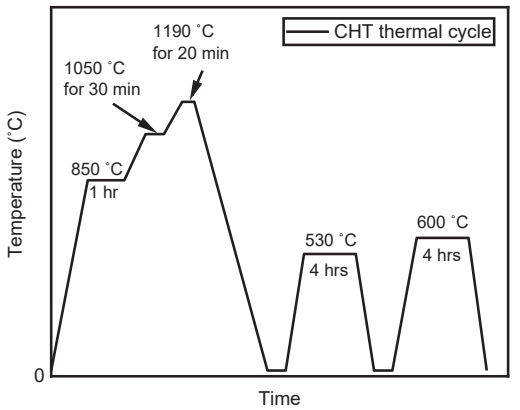

Figure 1: The CHT thermal cycle.

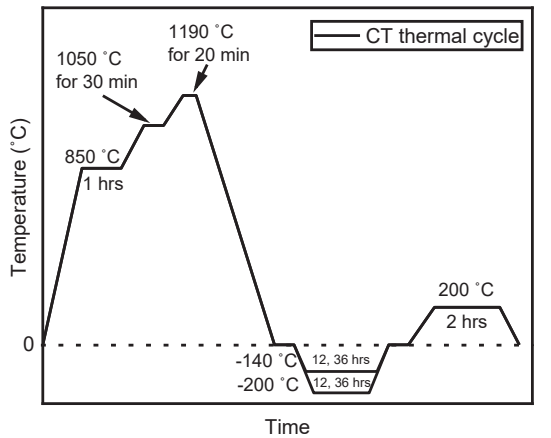

Figure 2: The cryogenic treatment thermal cycle (both SCT and DCT).

2.2 *Treatment conditions*

Table 2: The CT treatment detail of the SKH51 specimens

CT Type	Nomenclature	CT Parameters		Tempering
		Temp.	Time	
SCT	SCT-12	–140 °C	12 h	200 °C for 2 h
	SCT-36	–140 °C	36 h	200 °C for 2 h
DCT	DCT-12	–200 °C	12 h	200 °C for 2 h
	DCT-36	–200 °C	36 h	200 °C for 2 h

SKH51 specimen referred to as the reference in this work was CHT treated, and the samples were austenitized at 1190 °C before quenching to room temperature within 60 min by using N_2 gas. Double tempering was employed, the first-tempering at 530 °C for 4 h and then the second-tempering at 600 °C for 4 h. This treatment aimed to transform the RA into fresh martensite at the first-tempering and transform the fresh martensite to tempered martensite at the second-tempering. The CHT treatment thermal cycle is illustrated in Figure 1.

All the specimens prepared for CT treatment were partially CHT treated prior to the CT treatment. The CT process studied in this research was divided into two types SCT and DCT, which were made after the quenching process. The specimens were cooled down to the target process temperature at a cooling rate of 1 °C /min, held at a constant temperature, and then brought back to 35 °C in the treatment chamber at the rate of approx. 1 °C/min in all CT processes. The tempering process was performed after the CT. The CT conditions studied in this research are shown in Table 2. The thermal cycle of CT in both SCT and DCT is illustrated in Figure 2.

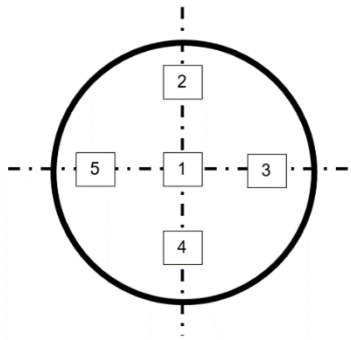

Figure 3: A schematic of the microstructure investigation area on the specimen's surface.

2.3 *Materials characterization*

2.3.1 Microscopy technique

An FEI Quanta 450 equipped with a LaB6 emitter Scanning Electron Microscopy (SEM) was used to investigate the backscattered images of the microstructure at a magnification of 5,000x. The specimens were etched with Villela acid (1 g picric acid, 5 mL hydrochloric acid, 100 mL ethanol) for 8 sec. A Light Optical Microscope (LOM) was also used to investigate the microstructure. There were five investigation areas (each with an area of 1150 μm^2), as illustrated in Figure 3. The carbide type, size, aspect ratio, and location were investigated. Over 500 carbide particles were analyzed in this work.

The Energy Dispersive Spectroscopy (EDS) technique was used to investigate the precipitation in

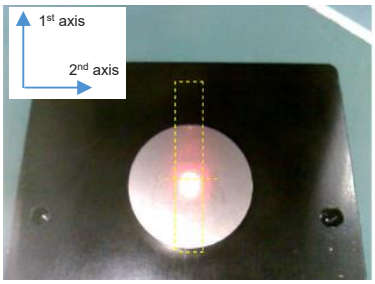

Figure 4: A schematic of the residual stress measurement area on the specimen's surface.

the SKH51 steel. The image analysis for the carbide size distribution of individual carbide and carbide aspect ratio was performed by using Digimizer image analysis software on the SEM micrographs. A similar technique was employed in many works [6], [12], [23].

The phase identification and the lattice parameter measurement of the matrix were carried out by using an Aeris bench-top X-ray diffractometer, PANalytical. A Cu-Kα with a wavelength of 1.5406 A˙ was used to analyze the samples. An X-ray beam, 1×1 mm, was used and measurement was made at the middle area of the sample's surface. Phase identification was achieved from the diffraction pattern [24]. Using the linear least-squares method, the lattice parameters were refined from the peak positions, assuming a BCC unit cell. The changes in the a-parameter of the martensite were calculated. The relative intensity ratio (RIR) method was used to calculate the phase fraction of all precipitations compared with the martensite matrix.

The residual stress on the specimen's surface was investigated by using a μ-X360 Residual Stress Analyzer (Pulstec Industrial Co., Ltd.) with a chromium (Cr) X-ray tube of 30 kV and 1.5 mA with 2 mm beam size and the cos α method. Note that the resolution depth was 10 μm into the surface. For each specimen, measurements were made in a two-directions along two perpendicular axes (denoted as 1st and 2nd axis) at the middle area. The testing schematic is illustrated in Figure 4. The technique was used to study the directional effect of the samples that had undergone different treatment processes [25].

2.4 *Hardness test*

A micro-Vickers hardness tester was used to evaluate the surface harness with a maximal load of 1000 gf and for 15 s, with five measurement points for each sample. Three samples were tested to confirm the results statistically. The micro-hardness measurement areas were distributed on the sample's surface corresponding to the microstructure investigation area, as illustrated in Figure 3.

2.5 *Wear test*

Dry sliding wear tests following the ASTM standard G99-05 with a 6 mm tungsten carbide ball and applied load of 5 N against the Ø20 × 5 mm samples were carried out on a computerized pin-on-disc wear testing machine (CSM Instrument model 01-03832 pin-on-disc test machine). All the samples were performed under dry condition at room temperature. The testing linear speed was 26 cm/s, while the testing distance was 1000 m. The wear volume loss was calculated in real-time based on the penetration depth of the indenter collected from the strain gauge sensor by assuming that the mass loss rate of the indenter was constant. The calculated results were confirmed by measuring wear volume loss after the test. The wear rate estimation was performed using the linear least-squares method in a steady-state regime [26].

3 Results and Discussion

3.1 *Microstructure analysis*

It can be seen in Figure 5 that the microstructure of the SKH51 comprises the matrix embedded with carbides, which are expected to be M_6C and MC carbide. Note that it is established that M_6C carbide and MC carbide are usually present in HSS [27]–[29]. The matrix of all these samples was expected to be tempered martensite and was confirmed by using the X-Ray Diffraction (XRD) technique.

The microstructure showed a significant difference after processing with different treatments. In the CHT, the grain boundary was noticed during the SEM investigations. However, it is not clearly observed in the image shown in Figure 5 (a). In the SCT (–140 °C), the clear grain boundary was clearly observed at 12 h but could not be found when holding the sample for 36 h, as shown in Figure 5(b) and (c), respectively. Micro-cracks occurred on the samples that underwent SCT for 36 h, as illustrated in Figure 5(c).

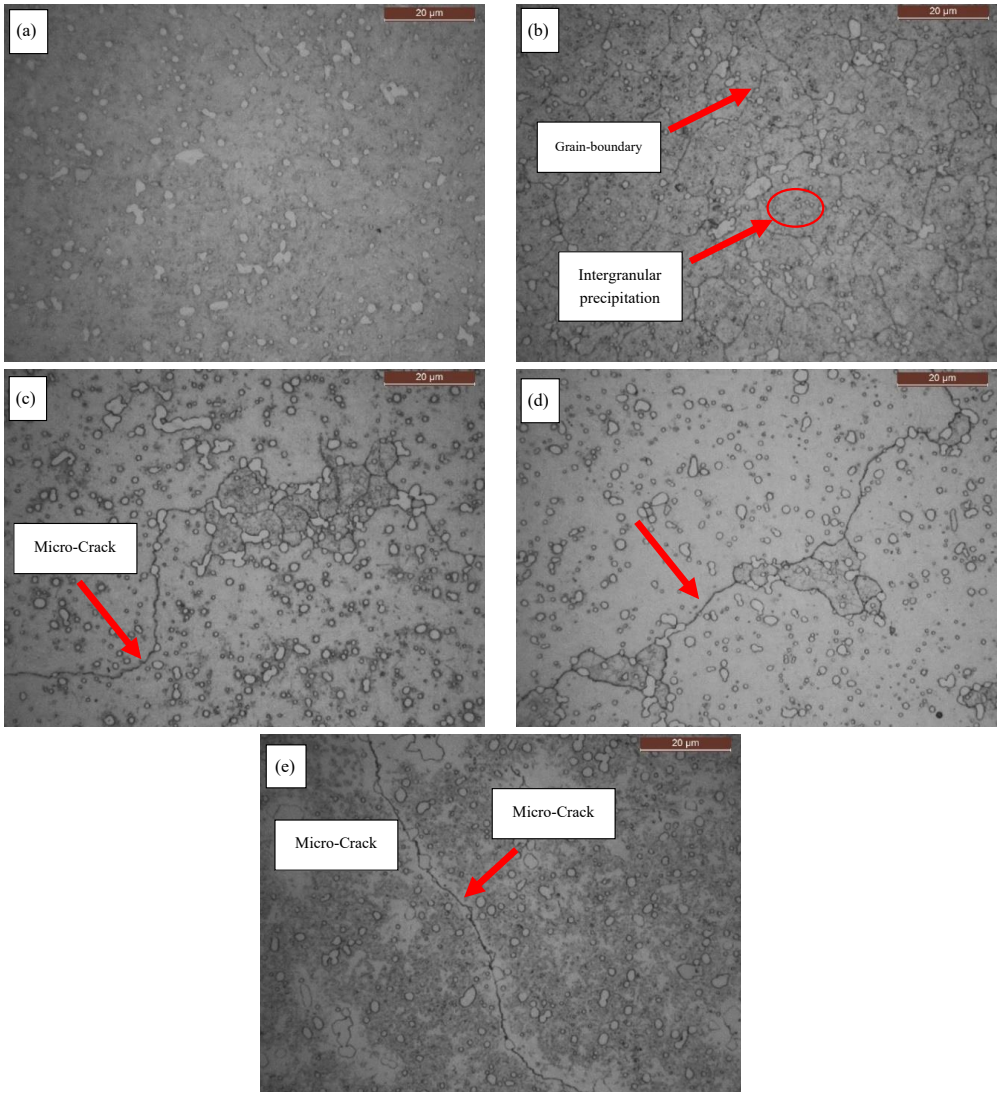

Figure 5: The image of SKH51 microstructure after undergoing different conditions: (a) CHT, (b) SCT-12, (c) SCT-36, (d) DCT-12 and (e) DCT-36 conditions (100x magnification).

In the DCT temperature (– 200 °C), micro-cracks were observed for 12 h of holding time [Figure 5 (d)]. The micro-cracks still appeared for the 36 hours holding time with the burn-remark on the martensite matrix without affecting the carbide, as shown in Figure 5(e). Note that all samples were etched with Villela acid at the same etching time (8 s). Normally, the etching acid will corrode the weakest regions in the microstructure, which usually refers to the grain boundary and the interface area between inclusion/matrix. High-alloy steels are more difficult to etch since some alloying elements, i.e., carbon (C), have very high resistance to the etching acid [30]. Moreover, the increase of internal stress contributes to the corrosion of steels [31]. The effect of cryogenic treatment on the internal stress of SKH51 will be discussed in the next topic. For this reason, the burn-remark of the samples may be caused by the change in microstructure as well as the increasing of the internal stress in the martensite matrix due to an application of DCT.

The micro-cracks would be developed and propagated if there was sufficient local stress generated in the direction of the crack opening. The residual stress can be produced due to the crystalline structure's contraction and expansion phenomena. The unequal contraction/expansion in the individual crystalline plane could cause crack opening stress. Moreover, the thermal expansion coefficient difference between the matrix, M_6C, and MC carbides can also make non-uniform contraction or expansion during the cooling and heating process, which can also lead to crack opening. These phenomena were investigated and confirmed by the following analysis. First, the lattice parameters of the matrix should show different contractions or expansion in the individual plane, which can be examined by XRD. Second, the measured residual stress should show a significant difference in different directions (two perpendicular directions were studied in this work). Finally, the Debye-Scherrer ring (D-S ring) diffracts from the crystalline structure in every plane should show a spotty or discontinuous ring. The occurrence of the micro-crack will be analyzed further using these concepts and will be discussed in more detail later. The similar phenomena has founded in Wannaprawat's work [32].

3.1.1 Carbide phase identification

The carbide's phase identification was carried out by scanning electron microscopy (SEM), as shown in Figure 6. The SEM micrograph shows the observable presence of reflective white particles and solid gray particles. These particles are different, and their different contrasts are due to their distinct atomic weights. Therefore, the SEM images suggested at least two different compounds precipitated in the metal specimens, as shown in Figure 6. Nevertheless, it is well-known that SKH51 steel is characterized by a martensitic matrix embedded in the MC and M_6C carbides [33]. It has been accepted that the reflective white particles are M_6C carbide, and solid gray particles are MC carbide [27], [34]. However, EDS was employed to confirm the type of carbide in this research. EDS analyses were carried on different reflective white and solid gray particles area of the different samples to investigate the composition.

An example of EDS analysis and results is shown

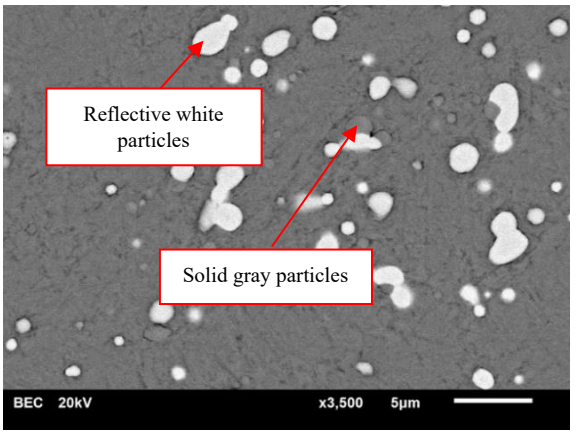

Figure 6: The microstructure of SKH51 after undergoing CHT.

in Figure 7. The results showed that the reflecting white particle comprises the iron (Fe), molybdenum (Mo), and tungsten (W) plus vanadium (V) at a low concentration, which is the theoretical element of M_6C carbide. The evidence can be seen in spectrum 2 and 3, respectively. The MC carbide is a non-stoichiometric vanadium carbide (VC) with some Mo and W dissolved, as shown in spectrum 1. It has to be noted that the value presented in Figure 7 is not the absolute value, but, it is normalized value to 100% in weight.

3.1.2 Carbide size analysis

The average size of individual M_6C and MC carbides was analyzed, and the results are presented in Table 3. In this work, the carbide size is defined as the maximal carbide particle length, while the carbide aspect ratio referred to the ratio between the longest axis (denoted as length) and shortest axis (denoted as width) of the carbide particle, as illustrated in Figure 8.

In the CHT condition, the average size of M_6C and MC carbide was 1.32 and 0.92 µm, respectively. The high variation in carbide size was observed in the CHT condition, which decreased dramatically in SCT and DCT conditions, as shown in Figure 9.

In SCT, the average M_6C carbide size increased from 1.15 to 1.29 µm, about 12% growth, after treating the sample for 12 and 36 h, respectively. Meanwhile, the MC carbide size showed no significant change due to SCT (from 0.86 to 0.87 µm after increasing the holding time), as demonstrated in Figure 9. The average

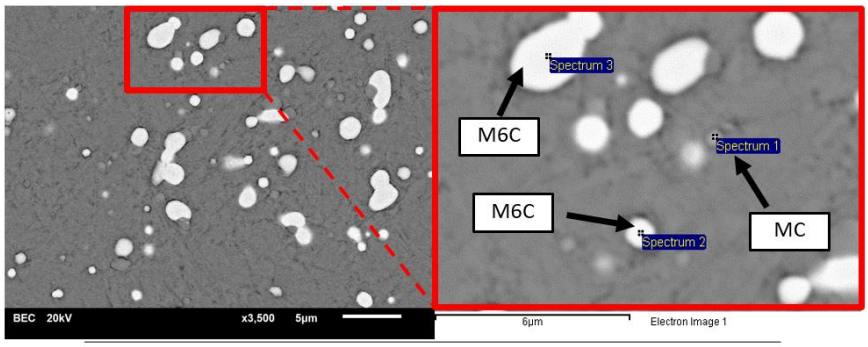

Spectrum	C	O	V	Cr	Fe	Mo	W	Total
Spectrum 1	**12.53**	-	**14.20**	3.86	45.12	10.55	13.74	100.00
Spectrum 2	5.67	2.29	2.22	3.47	**40.70**	**17.57**	**28.08**	100.00
Spectrum 3	4.95	1.71	2.87	3.00	**28.94**	**23.71**	**34.80**	100.00

Figure 7: Microstructure of SKH51 and carbide analysis using the EDS technique and the EDS results of SKH51 (%wt).

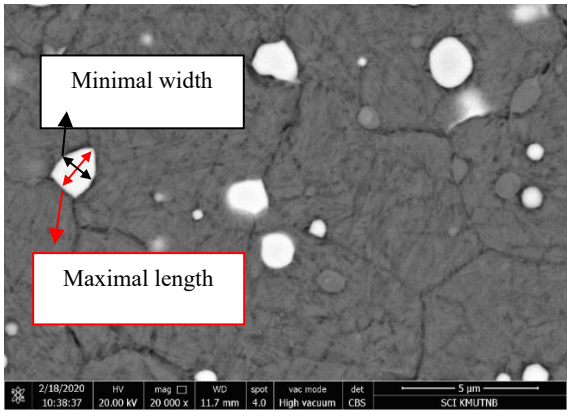

Figure 8: Image of a carbide particle showing the maximal length and minimal width.

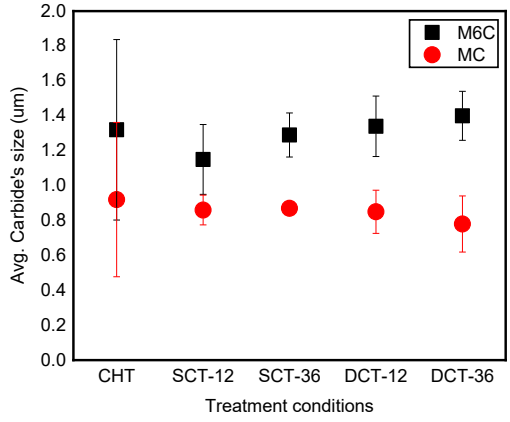

Figure 9: The average size of M6C and MC carbide after undergoing different treatment conditions.

size of the carbides in the SCT samples appeared smaller than those in the CHT samples for both M_6C and MC carbides. The average sizes of the M_6C carbide found for SCT-12 and SCT-36 cases were smaller than that in the CHT by up to 13% and 2%, respectively. The size of the MC carbide in the SCT samples was smaller than that found in the CHT specimens by about 6% for both the SCT-12 and SCT-36 samples. It can be seen that the SCT results in fine precipitation of M_6C and MC carbide.

In the DCT, the average M_6C carbide size was slightly increased from 1.34 to 1.40 μm (only 5%) after treating the sample for 12 and 36 hours of holding time, respectively. The MC carbide size changed from 0.85 to 0.78 μm or about 8% change due to the increase in the holding time. The average size of the M_6C carbides in the DCT samples was larger than that observed in the CHT specimens, i.e. up to 2% and 6% increase with the DCT-12 and DCT-36, respectively. The size of the MC carbide in

the DCT was significantly smaller than that found in the CHT cases, i.e. up to 8% and 15% for DCT-12 and DCT-36 conditions, respectively. The results inferred that the precipitation and growth mechanism of the carbide in the DCT region was different between the 12 and 36 h process time conditions. In the DCT-12, fine precipitation of M_6C and MC carbide was observed. While, in the DCT-36, significant growth of M_6C and size reduction of MC carbide was observed.

The process time effect will be discussed in this section. In the 12 hours holding time, the average size of the M_6C carbide was 1.15 µm when subjected to the SCT temperature (–140 °C) while the M_6C carbide size was 1.34 µm with DCT temperature (–200 °C). In other words, the DCT temperature (–200 °C) can increase the average size of M_6C by up to 16% compared to the SCT condition at 12 h holding time. The average size of the MC in the SCT condition was 0.86, while the MC size in the DCT condition was 0.85 µm (approx. 1% difference).

In the 36 h holding time, the average M_6C carbide was 1.29 µm for the SCT condition, while the average size of the M_6C carbide was 1.40 µm for the DCT condition. It can be seen that the carbide size increased by 8% after performing the DCT temperature (–200 °C) compared to the SCT condition. For the MC, the average size for the SCT condition was 0.87, while the MC size for the DCT condition was only 0.78 µm (10% difference).

The growth of M_6C carbide can be observed in both the SCT and DCT regions by increasing the holding time. The M_6C carbide growth in this research may be caused by the bonding of M_6C carbide with the ejected interstitial atom resulting from lattice structure contraction and expansion. Moreover, it could be observed that the M_6C carbide was usually at the grain boundary, where the ejected atoms could easily move due to its low surface energy.

Table 3: The average size of individual M_6C and MC carbide that undergone different treatment conditions (µm)

Carbide Types	CHT	SCT-12	SCT-36	DCT-12	DCT-36
M_6C	1.32	1.15	1.29	1.34	1.40
MC	0.92	0.86	0.87	0.85	0.78

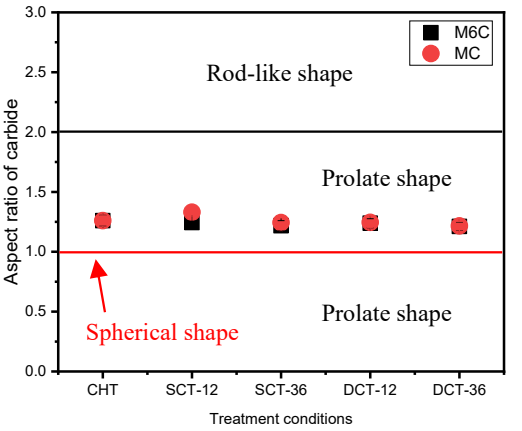

Figure 10: The aspect ratio of M_6C and MC carbide after undergoing different treatments.

3.1.3 Carbide shape analysis

The conventional definition of the aspect ratio refers to the longest axis (length) divided by the shortest axis (width) of the studied objects, as illustrated in Figure 8 [35], [36]. Therefore, the aspect ratio = 1 corresponds to a spherical shape, the aspect ratio > or the aspect ratio < 1 corresponds to a prolate shape and the aspect ratio > 2 corresponds to a rod-like shape [37]. The carbide's shape analysis in this research was performed by investigation of the aspect ratio of the individual type of carbides in SKH51. The aspect ratio reported in Figure 10 is a ratio between the maximal length (longest axis) and width (shortest axis) of the carbides.

The results were averaged from over 500 carbide particles. The results showed that the average aspect ratio of M_6C and MC carbides in this research was in the prolate shape region for every treatment condition.

3.1.4 X-Ray Diffraction spectroscopy (XRD)

The diffraction pattern of the specimens post treated conditions is shown in Figure 11(a) and (b).

The main diffraction peak of the matrix, M_6C and MC carbide, was shown in every treating condition, as shown in Figure 11(a). All the samples could be proved to be a Body-centered cubic (BCC) martensite, since the tetragonal lattice parameters a and c cannot be distinguished [38], as illustrated in Figure 11(b). The diffraction peak of the BCC martensite (110),

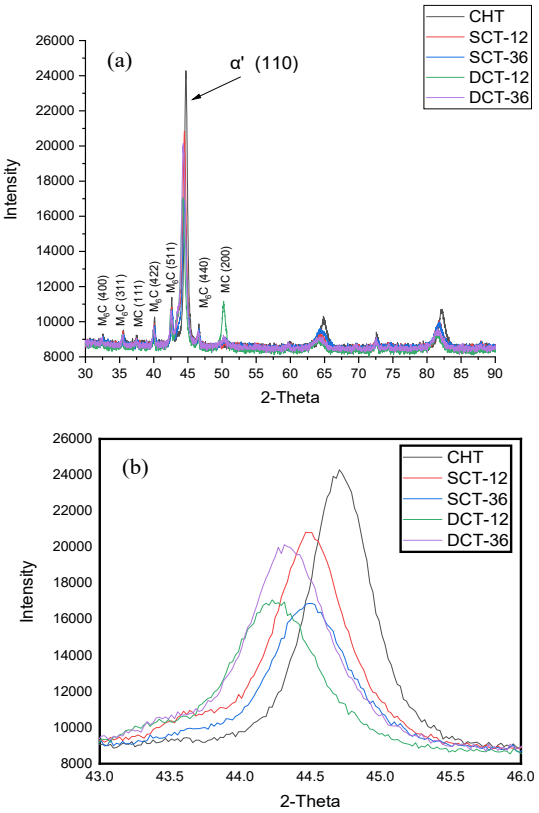

Figure 11: (a) The XRD pattern of the SKH51 specimens post treated conditions. (b) The XRD pattern of the martensite (110).

as illustrated in Figure 11(b), shows the significant change in the peak positioning due to the contraction and extraction of the lattice parameters as an effect of the cryogenic treatment.

3.1.5 Lattice parameters

The lattice parameters (a-parameters) of the BCC martensite matrix were analyzed by using Equation (1), where d is the d-spacing and hkl are miller indices. The average a-parameters is showed in Figure 12. This shows the average a-parameters of (110), (200), and (211) peaks of all treatment conditions.

$$a = d \times \sqrt{h \times k \times l} \quad (1)$$

In the CHT, the average a-parameters of BCC martensite were 0.3574 nm. The average a-parameters

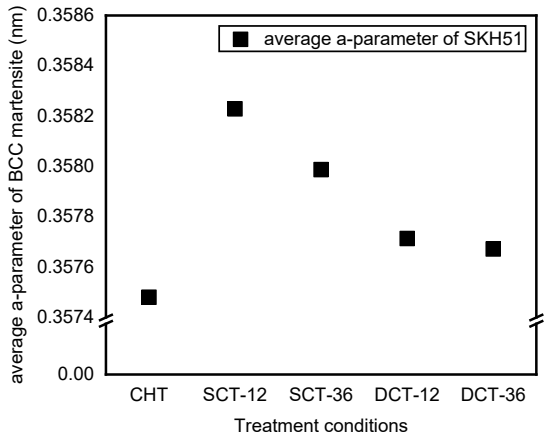

Figure 12: The average a-parameter of BCC martensite post different treatment conditions.

of the reference CHT seemed lower than the samples post CT, as shown in Figure 12. However, the dramatic difference in the a-parameters of the individual plane could be observed, as seen in Figure 13(a)–(c). This high difference in the individual plane can cause non-homogeneous distribution of the martensite's plane, where cab negatively affects the wear resistance of the material.

In the SCT temperature (–140 °C), the average a-parameters of the BCC martensite decreased dramatically from 0.35823 to 0.35799 nm by increasing the holding time. This phenomenon also occurred in the DCT condition (–200 °C). The longer holding time decreased the average a-parameters from 0.35771 to 0.35767 nm. At the 12 h holding time, the DCT temperature (–200 °C) showed significantly lower in the average a-parameters from 0.35823 to 0.35771 nm compared to the SCT temperature (–140 °C). Also, in the 36 h holding time condition, the average a-parameters decreased 0.35771 nm in the SCT temperature compared to 0.35767 nm in the DCT temperature.

It can be seen that the average a-parameters of the BCC martensite appeared to decrease with the increase in driving force (lower treatment temperature and longer holding time). It has to be noted that the decrease in the a-parameters resulted in lower carbon content in the martensite structure [38], [39]. Hence, the corrosive resistance of the BCC martensite matrix was decreased dramatically, resulting in the burn-mark after etching, as illustrated in Figure 5(e) previously,

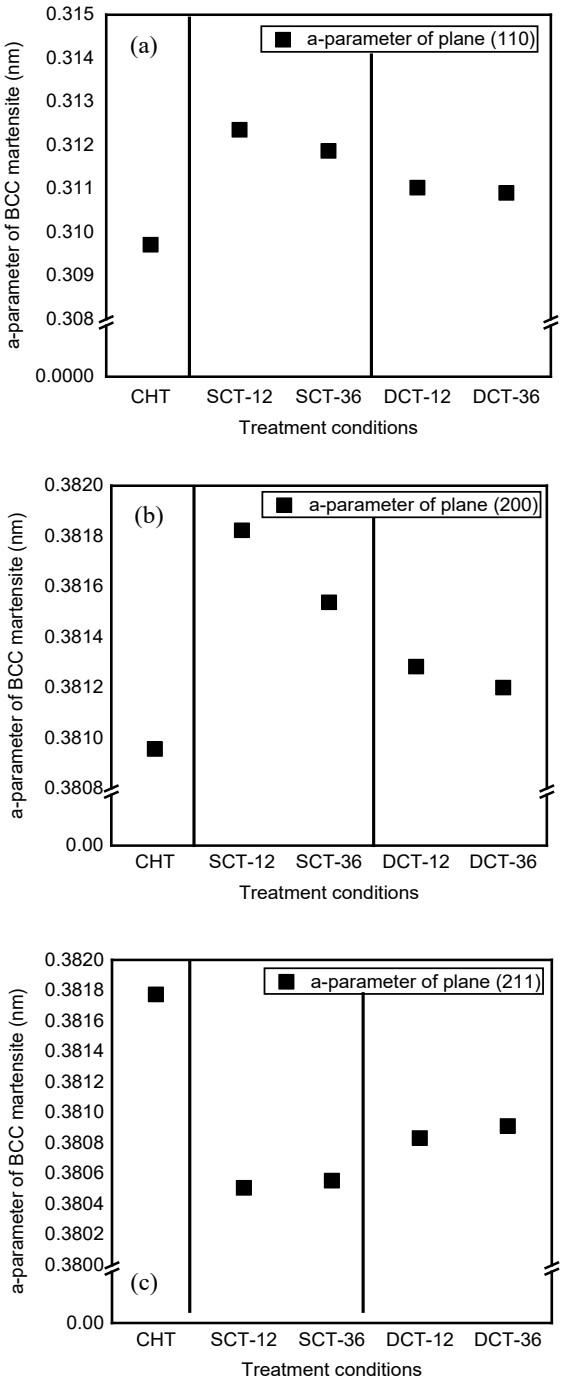

Figure 13: The a-parameter of the individual plane in BCC martensite structure post different treatment conditions, (a) plane (110) and (b) plane (200) and (c) plane (211).

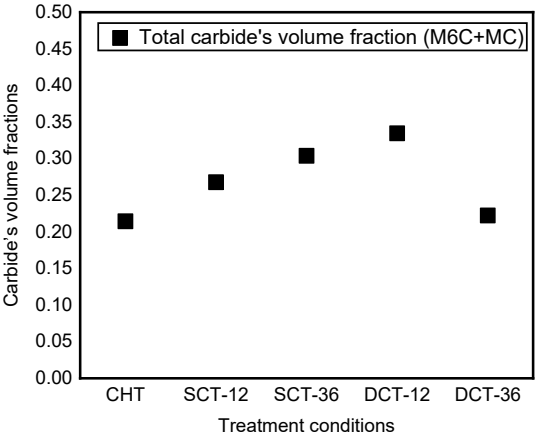

Figure 14: The total volume fraction of carbide (M_6C+MC) in the SKH51 steels post different treatment conditions.

which was expected to experience the highest driving force induced condition. Although the CHT samples reported the lowest a-parameters compared to those of the CT conditions, the volume fraction of the carbides was not as high as the sample that underwent the CT condition. This phenomenon could mean that the carbon atom was still placed in the interstitial atom positions and marked the martensite matrix to have better corrosion resistance than the DCT-36 condition. For this reason, the microscopic structure of SKH51 under the CHT condition could resist the etching acid better than the DCT-36 condition, and the burn-mark was invisible.

3.1.6 Volume fraction of carbides

The total carbide volume fraction (M_6C+MC) in the SKH51 steel is illustrated in Figure 14 and Table 4. The relative intensity ratio (RIR) method was used to analyze the volume fraction of carbide. For the CHT, the total volume fraction of carbide (M_6C+MC) was 0.21, which is lower than that found for any other CT samples.

In the SCT (–140 °C), the total volume fraction (M_6C+MC) of SKH51 steel increased from 0.27 to 0.30 when increasing the holding time from 12 h to 36 h or about a 10% increase. This phenomenon confirmed the reduction of the BCC martensite lattice structure, as previously discussed. The ejected carbon atoms from the matrix structure can become secondary carbide

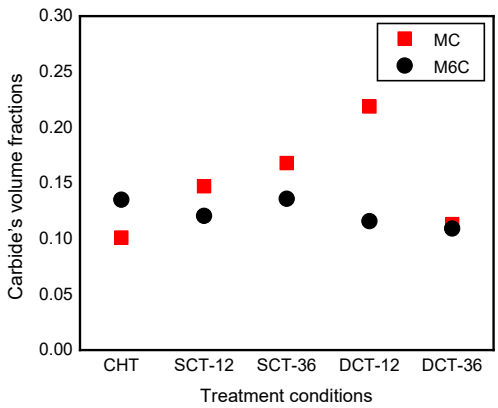

Figure 15: The individual M_6C and MC carbide's volume fraction in the SKH51 steel.

(MC carbide) precipitated in the samples, as shown in Figure 14. This phenomenon was also founded in Jurci *et al.* work's [23]. Increasing the MC carbide volume fraction raised the total carbide volume fraction in the samples. This phenomenon has been discussed among researchers [39], [40]. However, for the DCT, a significant drop of the carbide's volume fraction occurred when the holding time was increased from 12 h to 36 h, as shown in Figure 14. This unclear phenomenon needs to be further analyzed together with the carbide size results illustrated in Figure 9 and the individual volume fraction of carbide shown in Figure 15. In the DCT condition (–200°C), it was clear that the secondary carbide precipitated as an effect of the DCT was MC carbide with the 12 h holding time. However, the total volume fraction of the carbide (M_6C+MC) dropped from 0.33 to 0.23 when increasing the holding time from 12 h to 36 h or about a 30% decrease.

In the DCT-36 condition, the results showed that the volume fraction of MC carbide was not significantly increased compared to that the other cryogenic conditions. In fact, the volume fraction of the MC carbide stayed at the same level as that CHT condition. This leads to the question of "where is the ejected carbon atom." The assumption was made that the ejected carbon atoms in the DCT-36 condition may cause the growth of the M_6C primary carbide instead of leading to precipitate more MC carbide like the other CT conditions. The growth of M_6C carbide in the DCT-36 condition can be observed in Figure 9. In the DCT-36 condition, the average a-parameters of this condition was 0.357672 nm, which was the lowest compared to the other CT conditions. The hypothesis was made that the carbon atoms in the BCC martensite structure were almost empty in the 12 h holding time and continued to empty with a longer period, i.e. 36 hours. For this reason, the average a-parameters showed a slight decrease from 12 to 36 h. Moreover, the burn-mark could be observed in this treatment condition since the matrix with low carbon content is usually weak against the etching solution, as shown in Figure 5(e). It highlights that the total carbide volume fraction (M_6C + MC) of this condition was 0.23, which is dramatically lower than the DCT condition at 12 h by up to 30%, as shown in Figure 14.

The average size of the M_6C carbide increased by 16% compared to that of the 12 h conditions with no significant change in the MC carbide type, Figure 9. The assumption was that when the carbon atoms were ejected from the lattice and stayed in the DCT condition for a sufficiently long time (36 h), the ejected carbon atoms seem not nuclei of a new carbide but moved together with dislocation into the grain boundary which the M_6C primary carbide usually located. The free carbon atoms could easily bond and lead to a growth of the carbide particle. For this reason, the overall volume fraction of carbide in this condition was just equal to that found for the CHT condition, but the size of M_6C increased dramatically. Based on this assumption, the lowest lattice contraction, i.e. SCT-12 condition, showed the fine inter-granular precipitation because the driving energy is not enough to move the ejected carbon atom so far.

Table 4: The volume fraction of individual M_6C and MC carbide

Carbide Types	CHT	SCT-12	SCT-36	DCT-12	DCT-36
M_6C	0.14	0.12	0.14	0.12	0.11
MC	0.10	0.15	0.17	0.22	0.11

3.1.7 Residual stress analysis

As previously discussed, the CT could lead to a contraction in the BCC martensite in-plane (110) and (200) while (211) presented the expansion in the lattice structure. This phenomenon normally distorts the BCC lattice, which usually increases the dislocation density and compressive residual stress. However, the individual plane's contraction and expansion phenomena can also

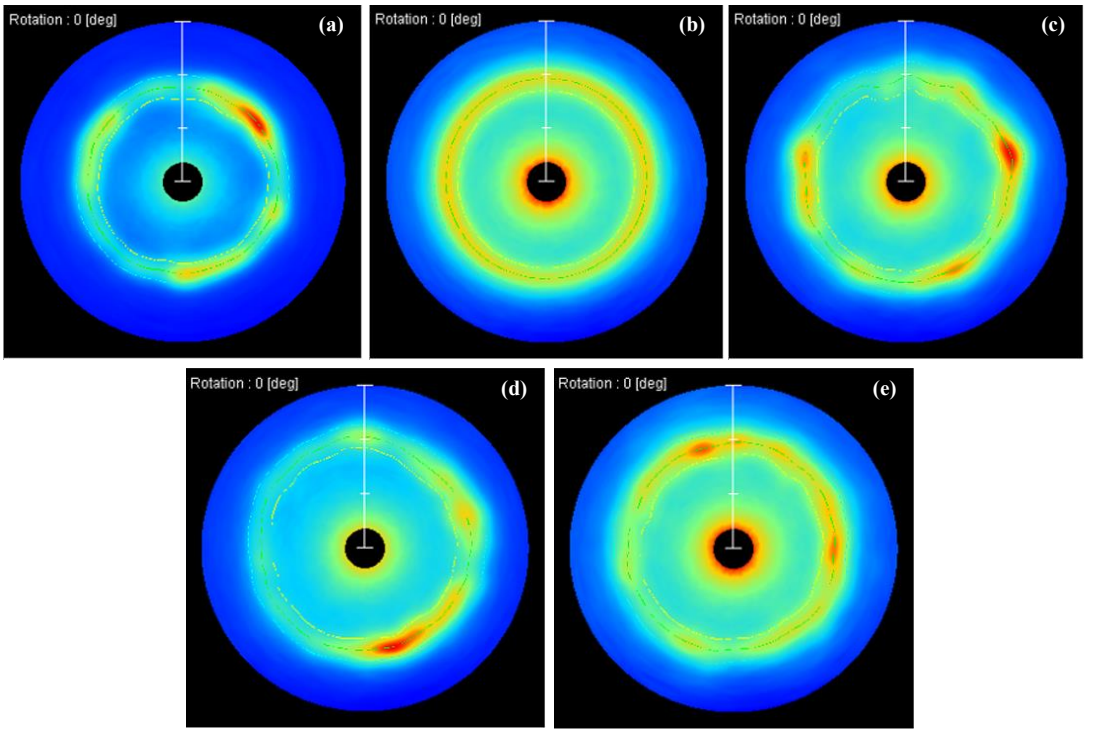

Figure 16: The Debye-Scherrer rings of the SKH51 specimens treated under different conditions: (a) CHT, (b) SCT-12, (c) SCT-36, (d) DCT-12, and (e) DCT-36.

cause the directional effect in the crystalline structure. The Debye-Scherrer method was used to analyze this phenomenon. The Debye-Scherrer ring (D-S ring) diffracts from the crystalline structure in every plane in the investigated area [25]. Hence, the smooth D-S ring can refer to the uniform distribution of the crystalline structure in every plane. The non-uniform distribution of the crystalline structure resulted in the spotty D-S ring or, in other words, the discontinuous D-S ring.

Figure 16 shows the D-S ring result from the SKH51 samples having undergone different treatment conditions. For the CHT conditions, this treatment is typically performed with double high-temperature tempering after the quenching process. Hence, the BCC martensite structure expands and contracts at least three times during CHT which could be challenging to make an even crystalline structure in every plane. The plane's unevenness in SKH51 having undergone CHT was observed and is illustrated in Figure 16(a).

In SCT (–140 °C), the 12 h condition showed a smooth D-S ring while the 36 h condition presented a discontinuous D-S ring. These results can be due to the contraction and expansion of the crystalline structure increased by increasing the driving force owing to the longer holding time, from 12 to 36 h. The plane's unevenness in the crystalline structure occurred strongly due to this phenomenon, as previously discussed. It should be noted that the 12 h SCT offered a more even structure compared with the CHT samples. This suggested that the effect of the low-temperature treatment process after quenching on microstructure unevenness due to the post double high-temperature tempering process conventionally employed could be resolved by using the SCT-12 condition. In DCT condition (–200 °C), the spotty D-S ring appears for both the 12 and 36 h holding times. The inhomogeneous distribution in the crystallite plane can be observed through this technique. It has to be noted that in all the treatment conditions micro-cracks were found in microstructures, illustrated in Figure 5, and showed discontinuity in the D-S ring.

The measured compressive residual stress is shown in Figure 17. The strong directional phenomena can be observed in the CHT, SCT-36, DCT-12, and

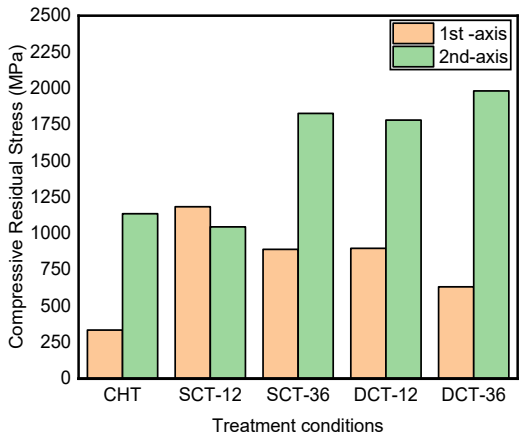

Figure 17: Compressive residual stresses of the SKH51 specimens undergone different treatment conditions in 1st and 2nd axis.

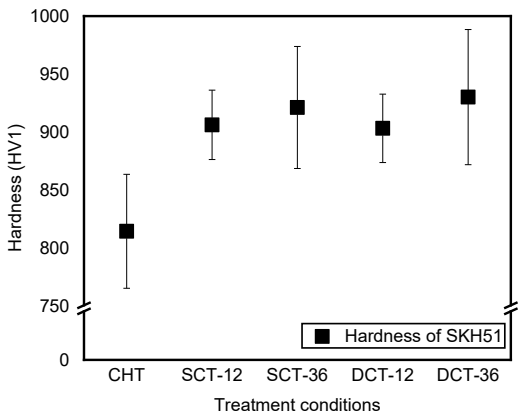

Figure 18: The average micro-hardness of SKH51 having undergone different treatment conditions.

DCT-36 conditions, suggesting significantly different compressive residual stress observed in two directions (1st and 2nd axis).

3.2 *Hardness*

Increases in micro-hardness level of CT treated specimens are reported in Figure 18. It was seen that the CT improved the average micro-hardness of SKH 51 from 814 to 930 HV1 or about 14% improvement compared to the CHT condition.

In the SCT, the average micro-hardness increased from 906 to 921 HV1 when increasing the SCT holding time from 12 to 36 h or only 2%. However,

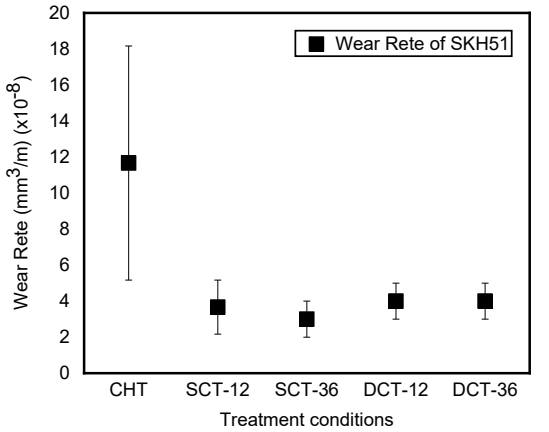

Figure 19: The average wear rate of SKH51 having undergone different treatment conditions.

the average micro-hardness of the samples having undergone SCT was about 12% higher than those of the CHT condition. The increasing of the MC carbide's volume fraction, fine precipitation of the carbide, and increasing compressive residual stress played an essential role in this improvement. In the DCT, the improvement of the micro-hardness from 903 to 930 was observed in the DCT-12 and DCT-36 conditions, respectively. Again, a small effect of holding time was observed, only a 3% increase in hardness was found with increasing the holding time from 12 to 36 h in the DCT region. However, the average micro-hardness of the sample having undergone DCT was about a 14% improvement compared to the CHT condition. The highest level of improvement corresponded to DCT-36 specimens. Such improvement was related to the increasing of compressive residual stress, the growth of M_6C primary carbide and fine precipitation of MC carbide, as previously discussed. This is expected to lead to the better wear resistance of the material having undergone CT treatment compared to CHT.

3.3 *Wear*

The improvement of the wear resistance in SKH51 having undergone different treatments is illustrated in Figure 19. The samples having undergone CT in both regions seemed to raise the wear resistance dramatically, as expected. However, the responsible mechanism for such improvement was expected to be different due to the different microstructure

modifications previously presented.

In the CHT, the wear rate of the samples in CHT was about three times higher than in the CT samples, although the average micro-hardness value of the CHT was lower than in the CT samples by about 14%. The mechanism behind this enormous improvement of wear resistance in the CT samples could be from a higher volume fraction of carbide with fine precipitation of carbide and the increasing of the compressive residual stress.

The formation of fine and very small carbide particles dispersed within the martensite provides more interfaces with the base martensite matrix. These interface increments provide more obstacles against dislocation movements and prevent the abrasive particles from penetrating into the matrix, improving the abrasion wear resistance. This phenomenon could be applied to describe the wear resistance mechanism of SCT-12, SCT-36, and DCT-12 conditions. In the DCT-36, the growth of the M_6C primary carbide governed the improvement of wear resistance by increasing the hard surface area against the abrasive particles. The compressive residual stress also played an important role in wear resistance improvement. The increase in compressive residual stress could decrease the effect of applied stress in the contact area. This could lead to a more challenging situation to generate wear debris, resulting in fewer abrasive wear particles.

4 Conclusions

In this work, the effect of SCT and DCT on SKH51 microstructure was studied. The hardness and wear resistance were also investigated. The obtained results suggested the followings.CT treatment could generate the contraction and expansion phenomena of the BCC martensite, which forces the carbon atom out from the lattice, resulting in the nucleation and growth of carbides in SKH51 material.The effect of the holding time on the microstructure modification of SKH51 steel in the SCT and DCT regions is different. In the SCT region, the increase in the holding time also increased the volume fraction of fine MC carbide due to the contraction and expansion phenomena of the lattice structure. But, in the DCT region, the increase in holding time grows the M_6C carbide instead of increasing the precipitation of the MC carbide.The CT can improve the wear resistance of SKH51 by up to 70% compared to the CHT condition. However, there are two main improvement mechanisms including: (i) the precipitation of the fine secondary carbide which was observed in the SCT-12, SCT-36 and DCT-12 conditions and (ii) the growth of M_6C carbide which increased the hard contact area between the samples and abrasive particle.

Acknowledgments

The authors gratefully thank the research grant supported by the Thailand Research Fund (TRF) under contract No. PHD60I0059 and the materials provided by Nichidai Thailand. The program of Mechanical Engineering (IDEME), The Sirindhorn International Thai-German Graduate School of Engineering (TGGS), King Mongkut's University of Technology North Bangkok (KMUTNB) are gratefully acknowledged for supporting with the testing apparatus.

References

[1] F. Meng, K. Tagashira, and H. Sohma, "Wear resistance and microstructure of cryogenic treated Fe-1.4Cr-1C bearing steel," *Scripta Metallurgica et Materialia*, vol. 31, no. 7, pp. 865–868, 1994, doi: 10.1016/0956-716x(94)90493-6.

[2] P. J. Singh, B. Guha, and D. R. G. Achar, "Fatigue life improvement of AISI 304L cruciform welded joints by cryogenic treatment," *Engineering Failure Analysis*, vol. 10, no.1, pp. 1–12, 2003, doi: 10.1016/s1350-6307(02)00033-x.

[3] F. Meng, K. Tagashira, and R. S. H. Azuma, "Role of eta-carbide precipitation in the wear resistance improvements of Fe-12Cr- Mo-V-1.4C tool steel by cryogenic treatment," *ISIJ International*, vol. 34, no. 2, pp. 205–210, 1994, doi: 10.2355/isijinternational.34.

[4] F. Cajner, D. Landek, H. Rafael, S. Šolić, and S. Kovačić, "Effect of deep cryogenic treatment on dilatometric curve and tribological properties of high speed steel," *International Heat Treatment and Surface Engineering*, vol. 6, no. 2, pp. 67–71, 2012. doi: 10.1179/1749514812z.000000000.

[5] A. Razavykia, C. Delprete, and P. Baldissera, "Correlation between microstructural alteration, mechanical properties and manufacturability after cryogenic treatment: A review," *Materials*,

vol.12, no. 20, 2019, doi: 10.3390/ma12203302.

[6] D. Das, A. K. Dutta, V. Toppo, and K. K. Ray, "Effect of deep cryogenic treatment on the carbide precipitation and tribological behavior of D2 steel," *Materials and Manufacturing Processes*, vol. 22, no. 4, pp. 474–480, 2007, doi: 10.1080/10426910701235934.

[7] S. A. Chopra and V. G. Sargade, "Metallurgy behind the cryogenic treatment of cutting tools: An overview," *Materials Today: Proceedings*, vol. 2, no. 4–5, pp. 1814–1824, 2015, doi: 10.1016/j.matpr.2015.07.119.

[8] F. Diekman, "Cold and cryogenic treatment of steel," *Steel Heat Treating Fundamentals and Processes*. Ohio: ASM International, 2013, pp. 382–386. https://doi.org/10.31399/asm.hb.v04a.a0005822

[9] N. S. Kalsi, R. Sehgal, and V. S. Sharma, "Cryogenic treatment of tool materials: A review," *Materials and Manufacturing Processes*, vol. 25, no. 10, pp. 1077–1100, 2010, doi: 10.1080/10426911003720862.

[10] A. Molinari, M. Pellizzari, S. Gialanella, G. Straffelini, and K. H. Stiasny, "Effect of deep cryogenic treatment on the properties of tool steel," *Journal of Materials Processing Technology*, vol. 118, no. 1–3, pp. 350–355, 2001, doi: 10.1016/s0924-0136(01)00973-6.

[11] V. Leskovsek and B. Ule, "Classic contributions: Cryogenic treatment Influence of deep cryogenic treatment on microstructure, mechanical properties and dimensional changes of vacuum heat-treated high-speed steel," *International Heat Treatment and Surface Engineering*, vol. 29, no. 7, pp. 155–161, 2002, doi: 10.1179/174951508x446385.

[12] S. Li, Y. Xie, and X. Wu, "Hardness and toughness investigations of deep cryogenic treated cold work die steel," *Cryogenics*, vol. 50, no. 2, pp. 89–92, 2010, doi: 10.1016/j.cryogenics.2009.12.005.

[13] S. Zhirafar, A. Rezaeian, and M. Pugh, "Effect of cryogenic treatment on the mechanical properties of 4340 steel," *Journal of Materials Processing Technology*, vol. 186, no. 1–3, pp. 298–303, 2007, doi: 10.1016/j.jmatprotec.2006.12.

[14] A. Idayan, A. Gnanavelbabu, and K. Rajkumar, "Influence of deep cryogenic treatment on the mechanical properties of AISI 440C bearing steel," *Procedia Engineering*, vol. 97, pp. 1683–1691, 2014, doi: 10.1016/j.proeng.2014.12.319.

[15] J. D. Darwin, L. D. Mohan, and G. Nagarajan, "Optimization of cryogenic treatment to maximize the wear resistance of 18% Cr martensitic stainless steel by Taguchi method," *Journal of Materials Processing Technology*, vol. 195, no. 1–3, pp. 241–247, 2008, doi: 10.1016/j.jmatprotec.2007.05.005.

[16] K. Moore and D. N. Collins, "Cryogenic treatment of three heat-treated tool steels," *Key Engineering Materials*, vol. 86–87, no. 47–54, pp. 47–54, 1993, doi: 10.4028/www.scientific.net/kem.86-87.47.

[17] R. F. Barron and C. R. Mulhern, "Cryogenic treatment of AISI-T8 and C1045 steels," *Advances in Cryogenic Engineering Materials*, pp. 171–179, 1980, doi: 10.1007/978-1-4613-9859-2_17.

[18] L. D. Mohan, S. Renganarayanan, and A. Kalanidhi, "Cryogenic treatment to augment wear resistance of tool and die steels," *Cryogenics*, vol. 41, no. 3, pp. 149–155, 2001. doi: 10.1016/s0011-2275(01)00065-0.

[19] F. J. D. Silva, S. D. Franco, Á. R. Machado, E. O. Ezugwu, and A. M. Souza, "Performance of cryogenically treated HSS tools," *Wear*, vol. 261, no. 5–6, pp. 674–685, 2006, doi: 10.1016/j.wear.2006.01.017.

[20] V. Leskovšek and B. Ule, "Classic contributions: Cryogenic treatment Influence of deep cryogenic treatment on microstructure, mechanical properties and dimensional changes of vacuum heat-treated high-speed steel," *International Heat Treatment and Surface Engineering*, vol. 3, no. 3–4, pp. 155–161, 2008, doi: 10.1179/174951508x446385.

[21] I. Alexandru, C. Picos, and G. Ailincai, "Contributions on the study of the increase of durability of the high-alloyed tool steels by thermal treatments at cryogenic temperatures," in *2nd International Congress on Heat Treatment of Materials*, 1982, pp. 573–579.

[22] R. Kelkar, P. Nash, and Y. Zhu, "Understanding the effects of cryogenic treatment on M2 tool steel properties," *Heat Treating Progress*, vol. 7, no. 5, pp. 57–60, 2007.

[23] P. Jurci, A. Bartkowska, M. Hudáková, M. Dománková, M. Caplovicová, and D. Bartkowski, "Effect of sub-zero treatments and tempering

on corrosion behaviour of Vanadis 6 tool steel," *Materials*, vol. 14, p. 3759, 2021, doi: https://doi.org/10.3390/ma14133759.

[24] N. Xu, G. P. Cavallaro, and A. R. Gerson, "Synchrotron micro-diffraction analysis of the microstructure of cryogenically treated high performance tool steels prior to and after tempering," *Materials Science and Engineering: A*, vol. 527, no. 26, pp. 6822–6830, 2010, doi: 10.1016/j.msea.2010.06.072.

[25] K. Tanaka, "X-ray measurement of triaxial residual stress on machined surfaces by the cosα method using a two-dimensional detector," *Journal of Applied Crystallography*, vol. 51, no. 5, pp. 1329–1338, 2018, doi: 10.1107/s1600576718011056.

[26] R. J. Bayer, *Mechanical Wear Fundamentals and Testing*. Florida: CRC Press, 2004.

[27] M. M. Serna and J. L. Rossi, "MC complex carbide in AISI M2 high-speed steel," *Materials Letters*, vol. 63, no. 8, pp. 691–693, 2009, doi: 10.1016/j.matlet.2008.11.035.

[28] X. Zhou, F. Fang, G. Li, and J. Jiang, "Morphology and properties of M2C eutectic carbides in AISI M2 steel," *ISIJ International*, vol. 50, no. 8, pp. 1151–1157, 2010, doi: 10.2355/isijinternational.50.

[29] H. Qua, B. Liao, L. Liu, D. Li, J. Guoa, X. Renc, and Q. Yang, "Precipitation rule of carbides in a new high speed steel for rollers," *Calphad*, vol. 36, pp. 144–150, 2012, doi: 10.1016/j.calphad.2011.06.006.

[30] H. E. Townsend, "Effect of alloying elements on the corrosion of steel in industrial atmospheres," *Corrosion*, vol. 57, no. 6, pp. 497–501, 2001, doi: 10.5006/1.3290374.

[31] V. G. Pleshivtsev, G. A. Filippov, Y. A. Pak, and O. V. Livanova, "Effect of carbon content and stressed state on the corrosion rate of pipe steel in heating systems," *Metallurgist*, vol. 53, no. 7–8, pp. 502–505, 2009, doi: 10.1007/s11015-009-9188-2.

[32] N. Wannaprawat and K. Tuchinda, "Influence of deep cryogenic treatment on microstructure, hardness, impact strength and wear of CuBeZr Alloy," *Chiang Mai Journal of Science*, vol. 48, no. 2, pp. 631–647, 2021.

[33] M. Boccalini and H. Goldenstein, "Solidification of high speed steels," *International Materials Reviews*, vol. 46, no. 2, pp. 92–115, 2001, doi: 10.1179/095066001101528411.

[34] H. F. Fischmeister, R. Riedl, and S. Karagöz, "Solidification of high-speed tool steels," *Metallurgical Transactions A*, vol. 20, no. 10, pp. 2133–2148, 1989, doi: 10.1007/bf02650299.

[35] D. Gantenbein, J. Schoelkopf, G. P. Matthews, and P. A. C. Gane, "Determining the size distribution-defined aspect ratio of rod-like particles," *Applied Clay Science*, vol. 53, no. 4, pp. 538–543, 2011, doi: 10.1016/j.clay.2011.01.034.

[36] X. Gao, T. Wang, and J. Kim, "On ductile fracture initiation toughness: Effects of void volume fraction, void shape and void distribution," *International Journal of Solids and Structures*, vol. 42, no. 18–19, pp. 5097–5117, 2005, doi: 10.1016/j.ijsolstr.2005.02.02.

[37] X. Yuan and Y. Ji, "Characterization and analysis of the aspect ratio of carbide grains in WC-Co composites," *RSC Advances*, vol. 8, no. 60, pp. 34468–34475, 2018, doi: 10.1039/c8ra03186j.

[38] V. A. Lobodyuk, Y. Y. Meshkov, and E. V. Pereloma, "On tetragonality of the martensite crystal lattice in steels," *Metallurgical and Materials Transactions* A, vol. 50, pp. 97–103, 2018, doi: 10.1007/s11661-018-4999-z.

[39] X. Zhou, D. Liu, W. L. Zhu, F. Fang, Y. Y. Tu, and J. Q. Jiang, "Morphology microstructure and decomposition behavior of M2C carbides in high speed steel," *Journal of Iron and Steel Research*, vol. 24, no. 1, pp. 43–49, 2017, doi: 10.1016/s1006-706x(17)30007-9.

[40] D. Das, A. K. Dutta, V. Toppo, and K. K. Ray, "Effect of deep cryogenic treatment on the carbide precipitation and tribological behavior of D2 steel," *Materials and Manufacturing Processes*, vol. 22, no. 4, pp. 474–480, 2007, doi: 10.1080/10426910701235934.